The Astrophysical Journal Supplement Series, 180:182–191, 2009 January 1 doi:10.1088/0067-0049/180/1/182

LABORATORY SPECTRA OF THE CO_2 BENDING-MODE FEATURE IN INTERSTELLAR ICE ANALOGUES SUBJECT TO THERMAL PROCESSING

D. W. White[1], P. A. Gerakines[1], A. M. Cook[2], and D. C. B. Whittet[2]
[1] Department of Physics, the University of Alabama at Birmingham, Birmingham, AL 35294-1170, USA; dwhite@uab.edu
[2] Department of Physics, Applied Physics, & Astronomy, Rensselaer Polytechnic Institute, Troy, NY 12180-3590, USA
Received 2008 May 13; accepted 2008 September 25; published 2008 December 24

ABSTRACT

The infrared absorption features of solid carbon dioxide have been detected by space-based observatories in nearly all lines of sight probing the dense interstellar medium (ISM). It has also been shown that the absorption feature of solid CO_2 near 658 cm^{-1} (15.2 μm) should be a sensitive indicator of the physical conditions of the ice (e.g., temperature and composition). However, the profile structure of this feature is not well understood, and previous laboratory studies have concentrated on a limited range of temperatures and compositions for comparisons with observed spectra from both the *Infrared Space Observatory* and the *Spitzer Space Telescope*. In the laboratory study described here, the infrared spectra of ices bearing H_2O, CH_3OH, and CO_2 have been measured with systematically varying compositions and temperatures that span the range of the values expected in the ISM. The mid-IR spectra (λ = 2.5–25 μm) were measured for 47 different ice compositions at temperatures ranging from ~5.5 K to evaporation, at 5 K intervals.

Key words: astrochemistry – ISM: abundances – ISM: molecules – methods: laboratory – molecular data

Online-only material: color figures and machine-readable table

1. INTRODUCTION

The compositions of icy materials in the interstellar medium (ISM) are typically studied by observing the absorption of starlight by dense interstellar clouds in the mid-infrared (mid-IR) spectral region, λ = 2.5–25 μm (Chiar et al. 1995). In dense cores, where particle densities can be ~10^3 cm^{-3} or higher, temperatures fall below 10 K and volatiles from the gas phase may form an icy grain mantle by surface reactions or by freezing out onto interstellar dust grains. Observations in the mid-IR (e.g., Gibb et al. 2000) have identified the absorption features of molecules such as H_2O, CH_3OH, CO, and CO_2 in many lines of sight at various abundance levels (usually dependent upon the local environment). The shapes of their infrared absorption profiles have shown that the icy grain mantles come in at least two phases: one dominated by H_2O, and one by nonpolar, weakly interacting species such as CO or CO_2 (Tielens et al. 1991; Chiar et al. 1995).

Before the launch of the *Infrared Space Observatory* (*ISO*), it was suspected that relatively large abundances of interstellar solid CO_2 would be found in environments exposed to processing radiation such as UV and cosmic rays (Whittet & Duley 1991; Weaver et al. 1994). This hypothesis was based on laboratory analog experiments that predicted the efficient production of CO_2 inside mixed ices containing H_2O and CO, two known components of icy grain mantles in dense clouds (Hagen et al. 1979; Sandford & Allamandola 1990). Analyses of the *ISO* Short-Wavelength Spectrometer (SWS) data revealed that CO_2 was present in virtually all lines of sight that passed through the dense phase of the ISM, with a typical abundance of 15%–25% relative to solid H_2O (e.g., de Graauw et al. 1996; Gerakines et al. 1999; Dartois et al. 1999; Boogert et al. 2000). No correlation with the ambient radiation field was found, indicating that radiative processing is not required for CO_2 formation. Comparisons of the *ISO*-SWS data with spectra from the laboratory also revealed that many interstellar solid CO_2 spectra closely resembled those of CO_2 in mixtures with H_2O and CH_3OH (Dartois et al. 1999; Ehrenfreund et al. 1999), where a principal variation between the best-fitting laboratory spectra for different interstellar lines of sight was the temperature of the ice mixture (Gerakines et al. 1999). This suggests that the presence of CH_3OH indicates thermal processing. Though other processes such as UV radiation are possible, a formation route to CO_2 in interstellar ices due to atom bombardment is explored with the authors' experiments.

Another unpredicted aspect of the observed interstellar CO_2 spectra lay in the observed profiles of the solid CO_2 absorption feature near $\tilde{\nu}$ = 658 cm^{-1} (λ = 15.2 μm). If the solid CO_2 was formed as predicted, by the energetic processing of an H_2O + CO ice mixture (in a ratio of ~10:1), one would expect to find the solid CO_2 in a matrix dominated by H_2O. However, the observed interstellar spectra of highly processed regions (such as regions near young stellar objects (YSOs)) typically contained the sharp, double-peaked structure indicative of a relatively pure CO_2 ice as well as a long-wavelength shoulder near 654 cm^{-1} most likely due to an interaction between CO_2 and CH_3OH (Ehrenfreund et al. 1998, 1999; Gibb et al. 2004). Laboratory analogues with the composition H_2O + CH_3OH + CO_2 (1:1:1) yielded the best spectral fits to all of these profile substructures (Ehrenfreund et al. 1999; Gerakines et al. 1999). Observations of abundant solid CO_2 were also made in quiescent clouds that are far from any source of energetic processing. This showed that other production routes are required (Whittet et al. 1998). Subsequent laboratory experiments have since shown that thermal processing and grain-surface phenomena are better candidates for understanding the origin and evolution of interstellar solid CO_2 (Moore et al. 2001).

The Infrared Spectrograph (IRS) instrument of the *Spitzer Space Telescope* has since permitted further study of the interstellar CO_2 spectrum near 658 cm^{-1} with a higher sensitivity but a lower spectral resolution than the *ISO*-SWS. With *Spitzer*, the 658 cm^{-1} absorption feature of solid CO_2 has been observed toward objects with much lower fluxes at this wavelength, such as protoplanetary disks (Pontoppidan et al. 2008), class-1

protostars (Watson et al. 2004), and field stars located behind quiescent regions of the dense ISM (Bergin et al. 2005; Whittet et al. 2007). These observations extend the range of observed environments, probing a range of ice compositions and temperatures significantly different from that observed by the *ISO*. It is also necessary to use laboratory spectra to classify the composition and temperature of these environments with greater precision than was available with prior laboratory data sets.

This work provides a systematic set of mid-IR spectra (focusing on the 700–600 cm^{-1} range) of low-temperature (5–180 K) thin films (2–6 μm in thickness) containing H_2O, CH_3OH, and CO_2. The composition of the films was systematically varied over a wide range that spans the types of environments expected in the dense ISM. A spectrum of each mixture was measured at each 5 K interval ranging from ~5.5 K until the evaporation of the ice sample (~100–180 K). It should be noted that this work is not intended to be a comprehensive database of all possible interstellar ice compositions. Though others have explored nonpolar ice components such as CO (e.g., Ehrenfreund et al. 1997; Pontoppidan et al. 2008), we are focusing on exploring the dependence of the 658 cm^{-1} profile on H_2O and CH_3OH concentrations, and the ice temperature. This study was motivated largely by the ability of $H_2O + CH_3OH + CO_2$ mixtures to reproduce the bending-mode profiles as observed by both *ISO* and *Spitzer* (e.g, Ehrenfreund et al. 1999; Gerakines et al. 1999). Though CH_3OH is not visible in many lines of sight, it still influences the 658 cm^{-1} feature significantly. These spectra are presented in order to make them available to the astronomical community for use in the interpretation of IR data from observatories such as *Spitzer*. They may be used to fit observational data as well as provide a better understanding of the structure of $H_2O + CH_3OH + CO_2$ ice mixtures and their dependence on temperature and composition.

2. EXPERIMENTS

The ice creation methods and the experimental system used in this study are the same as those in a previous study by Gerakines et al. (2005). Gases were prepared inside a vacuum manifold and vapor-condensed onto an infrared transmitting substrate (CsI) mounted in the vacuum chamber ($P \approx 3\times10^{-6}$ mm Hg at room temperature). The substrate is cooled by a closed-cycle helium refrigerator (Air Products) to a temperature of about 5.5 K. The temperature of the substrate is continuously monitored by a chromel-Au thermocouple and is adjustable by a resistive heater element up to room temperature. The chamber that houses the substrate is accessible to laboratory instruments through four ports. Two of these ports have windows composed of KBr, allowing transmission of the infrared beam of the spectrometer. One of the ports contains a window composed of MgF_2 to enable ultraviolet photolysis of the ice samples (this option was not used for the experiments described in this research), while the fourth port has a glass window and is used to allow the measurement of ice thickness during deposit using laser interference fringes. The sample chamber is positioned within the sample compartment of a Fourier Transform InfraRed (FTIR) spectrometer (ThermoMattson Infinity Gold) so that the spectrometer's IR beam passes through the KBr windows and CsI substrate. Mid-IR spectra were obtained in the wavelength range from 4500 to 400 cm^{-1} (2.2–25 μm), with a resolution of 1 cm^{-1}.

A bulb containing the gas to be condensed was prepared on a separate vacuum manifold and then connected to the high-vacuum system by a narrow tube through a needle valve, which controlled the gas flow into the high-vacuum system. The tube is positioned to release the gases just in front of the cold substrate window. The thickness of the sample was determined by monitoring the interference of 650 nm laser light passing perpendicularly through the sample during growth. Gases were deposited at a rate of about 1–5 μm hr^{-1}. The gases used and their purities are as follows: CO_2 (Matheson, 99.8%), H_2O (distilled by freeze-thaw cycles under vacuum), and CH_3OH (distilled by freeze-thaw cycles under vacuum). H_2O and CH_3OH were purified by freezing with liquid N_2 under vacuum and pumping away the more volatile gases while thawing.

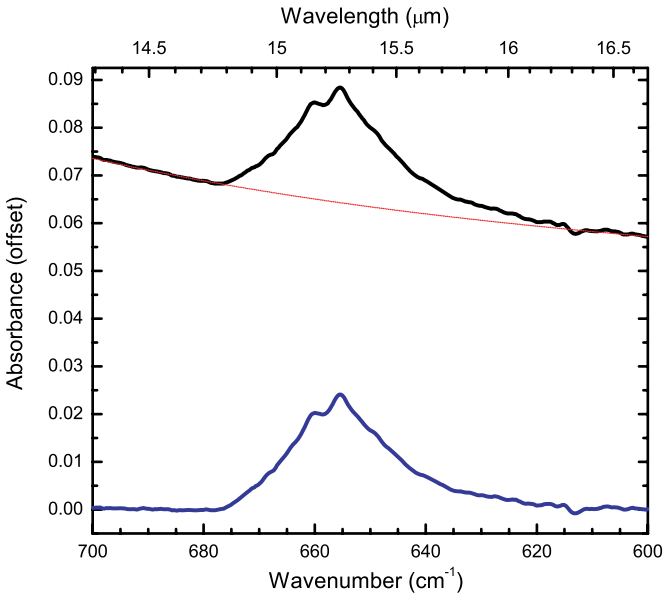

Figure 1. Demonstration of the baseline removal process using a third-order polynomial fit to the spectral regions near the CO_2 feature in a spectrum of H_2O + CO_2 (2:1) at 115 K. Top spectrum: original spectrum. Dotted line: polynomial fit. Bottom spectrum: spectrum after subtraction.

(A color version of this figure is available in the online journal.)

Table 1
Observed Peak Positions and Widths

Temperature (K)	$\tilde{\nu}(1)$ (cm^{-1})	$\tilde{\nu}(2)$ (cm^{-1})	$\Delta\tilde{\nu}(1)$ (cm^{-1})	$\Delta\tilde{\nu}(2)$ (cm^{-1})
Pure CO_2				
5.5	660	655	4	3
10	660	655	4	3
15	660	655	4	3
20	660	655	4	3
25	660	655	4	3
30	660	655	4	3
35	660	655	4	3
40	660	655	4	3
45	660	655	3	3
50	660	655	3	2
55	660	655	3	3
60	660	655	3	3
65	660	655	3	3
70	660	655	3	2
75	660	655	2	2
80	660	655	2	2

Note.
[a] The 658 cm^{-1} feature of CO_2 was not distinguishable in this ice deposit.
(This table is available in its entirety in a machine-readable form in the online journal. A portion is shown here for guidance regarding its form and content.)

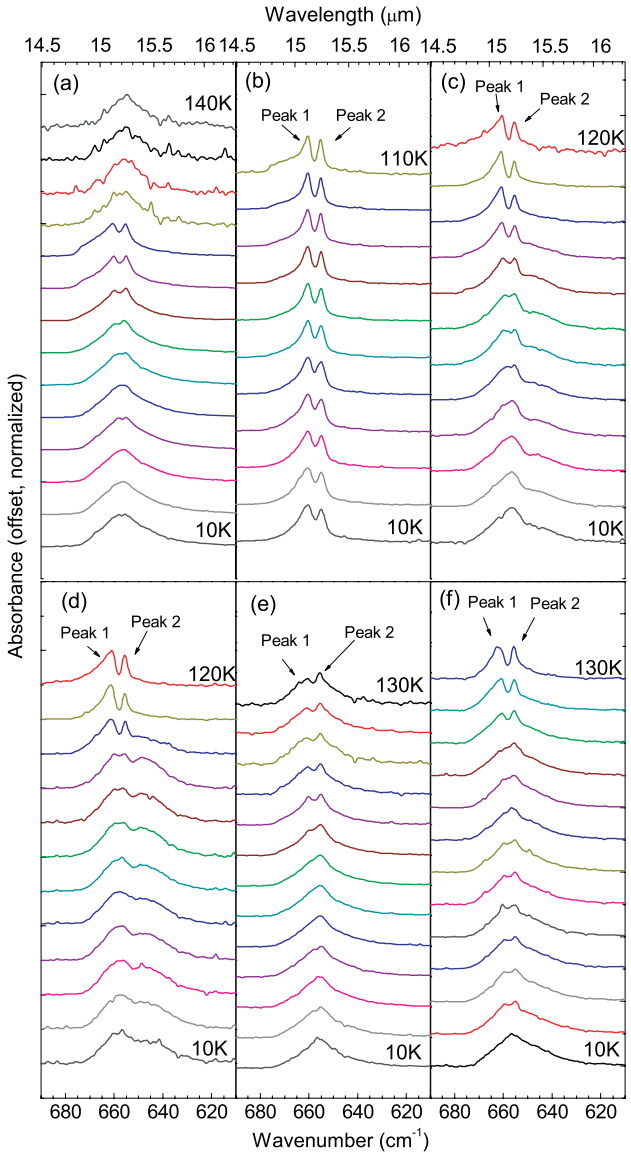

Figure 2. IR spectra, from 690 to 610 cm^{-1} (14.5 to 16.3 μm), of a laboratory ice mixture containing H_2O, CH_3OH, and CO_2 with more than 33% CO_2. All ice samples were heated at 1 K $minute^{-1}$ from 5 K to evaporation. Temperature intervals of 10 K are shown. (a) $H_2O + CO_2$ (1:1), (b) $CH_3OH + CO_2$ (0.1:1), (c) $CH_3OH + CO_2$ (0.5:1), (d) $CH_3OH + CO_2$ (1:1), (e) $H_2O + CH_3OH + CO_2$ (0.7:0.1:1), and (f) $H_2O + CH_3OH + CO_2$ (0.9:0.5:1).

(A color version of this figure is available in the online journal.)

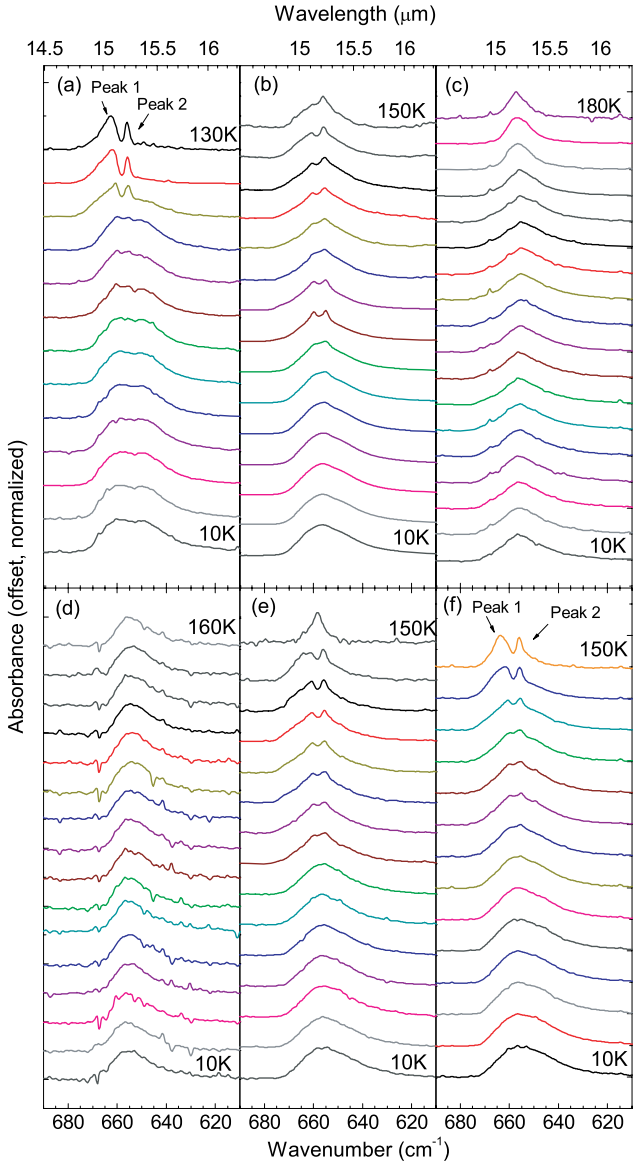

Figure 3. IR spectra, from 690 to 610 cm^{-1} (14.5 to 16.3 μm), of a laboratory ice mixture containing H_2O, CH_3OH, and CO_2 with more than 33% H_2O. All ice samples were heated at 1 K $minute^{-1}$ from 5 K to evaporation. Temperature intervals of 10 K are shown. (a) $H_2O + CH_3OH + CO_2$ (1:0.9:1), (b) $H_2O + CO_2$ (1.9:1), (c) $H_2O + CO_2$ (5.7:1), (d) $H_2O + CO_2$ (15:1), (e) $H_2O + CH_3OH + CO_2$ (2.1:0.1:1), and (f) $H_2O + CH_3OH + CO_2$ (1.8:0.5:1).

(A color version of this figure is available in the online journal.)

After each ice mixture was deposited at ~5.5 K, the substrate was then heated at a rate of 1 K $minute^{-1}$. Spectra were recorded at each 5 K interval at a resolution of 1 cm^{-1} until the sample evaporated. Additional scans were recorded in 10 K steps above 150 K to evaporation if the 658 cm^{-1} CO_2 feature remained at these higher temperatures. The evaporation temperature for any given ice was dependent upon its composition; for mixtures composed predominantly of CO_2, evaporation occurred near a temperature of 70 K, while those composed mainly of CH_3OH evaporated near 120 K and those with H_2O, near 180 K. The absorbance spectrum for each mixture and temperature was subsequently analyzed. The broad, strong libration mode peak due to H_2O and CH_3OH was removed to isolate the 658 cm^{-1} CO_2 profile. This was done by fitting a polynomial of order 1–3 underneath the CO_2 bending mode and then subtracting the fit from each of the spectra. An example is shown in Figure 1. Each spectrum was then normalized to its maximum absorbance value between 730 and 550 cm^{-1} (13.7 and 18.2 μm) for ease of comparison. A total of 47 mixtures of $H_2O + CH_3OH + CO_2$ were studied. The compositions used in these experiments are listed in Table 1 along with the peak positions and full widths at half-maximum (FWHM) of the 658 cm^{-1} features. Column density calculations were performed on the O–H stretching mode at 3280 cm^{-1} for H_2O, the C–O stretching mode at 1041 cm^{-1} for CH_3OH, and the C=O stretching mode at 2342 cm^{-1} for CO_2. Band strengths used in the calculations were obtained from Gerakines et al. (1995), Hudson & Moore (1999), and Oberg et al. (2007). The band strengths used for the C=O stretching mode of CO_2 and the O-H stretch mode of H_2O were dependent upon the composition of the mixture, in accordance with the results of Gerakines et al. (1995). The band strengths

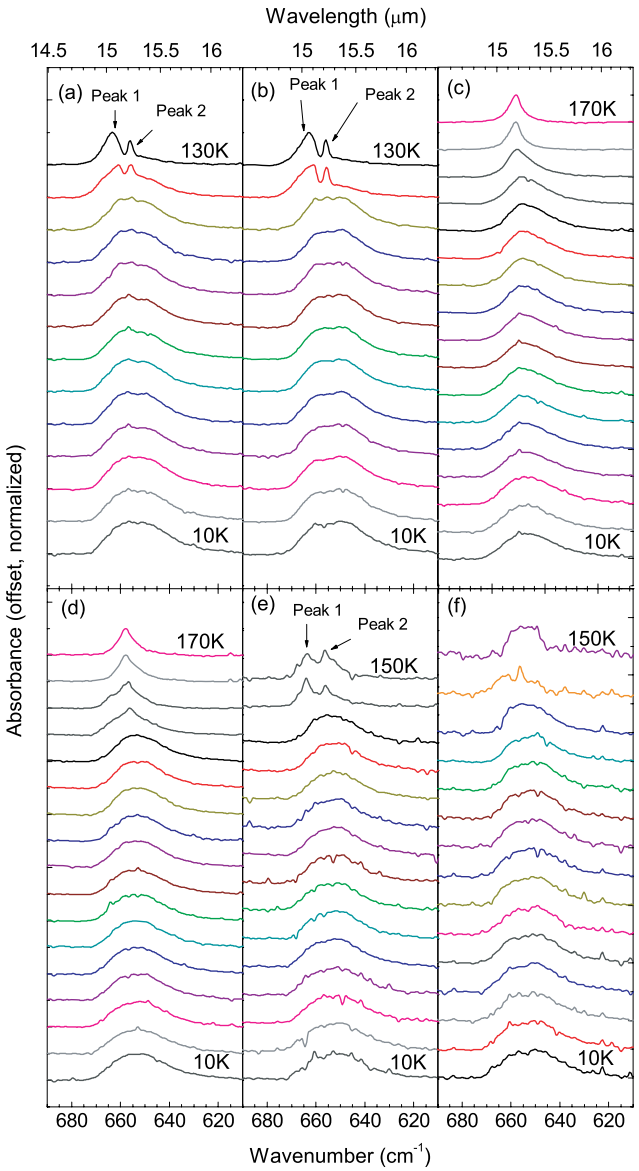

Figure 4. IR spectra, from 690 to 610 cm^{-1} (14.5 to 16.3 μm), of a laboratory ice mixture containing H_2O, CH_3OH, and CO_2 with more than 33% H_2O. All ice samples were heated at 1 K $minute^{-1}$ from 5 K to evaporation. Temperature intervals of 10 K are shown. (a) H_2O + CH_3OH + CO_2 (2:0.9:1), (b) H_2O + CH_3OH + CO_2 (2.2:1.5:1), (c) H_2O + CH_3OH + CO_2 (6.1:0.2:1), (d) H_2O + CH_3OH + CO_2 (5:1.1:1), (e) H_2O + CH_3OH + CO_2 (5:1.6:1), and (f) H_2O + CH_3OH + CO_2 (4.5:2.4:1).

(A color version of this figure is available in the online journal.)

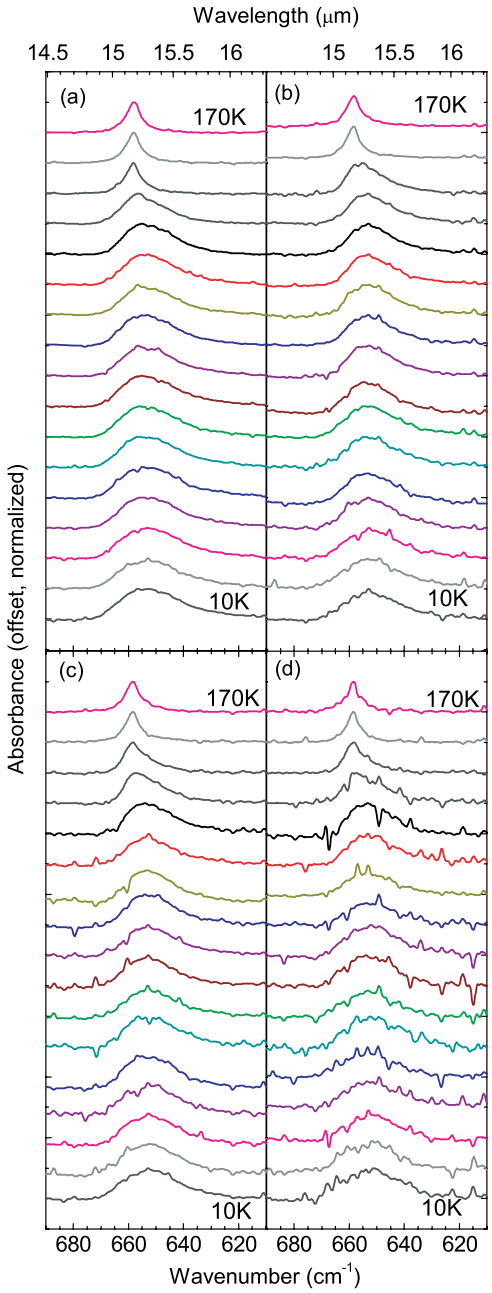

Figure 5. IR spectra, from 690 to 610 cm^{-1} (14.5 to 16.3 μm), of a laboratory ice mixture containing H_2O, CH_3OH, and CO_2 with more than 33% H_2O. All ice samples were heated at 1 K $minute^{-1}$ from 5 K to evaporation. Temperature intervals of 10 K are shown. (a) H_2O + CH_3OH + CO_2 (5.3:0.6:1), (b) H_2O + CH_3OH + CO_2 (11:0.2:1), (c) H_2O + CH_3OH + CO_2 (14:0.8:1), and (d) H_2O + CH_3OH + CO_2 (13:1.4:1).

(A color version of this figure is available in the online journal.)

used were as follows: $A(3280\,cm^{-1}) = 1.8 \times 10^{-16}$ cm $molec^{-1}$ for mixtures with less than 30% CO_2, $A(3280\,cm^{-1}) = 2.0 \times 10^{-16}$ cm $molec^{-1}$ for mixtures with more than 30% CO_2, $A(1041\,cm^{-1}) = 1.5 \times 10^{-17}$cm $molec^{-1}$, and $A(2342\,cm^{-1}) = 7.6 \times 10^{-17}$ cm $molec^{-1}$. In mixtures where the absorbance of the C = O stretching mode was greater than 1 (and hence unreliable for column density estimation), the much weaker C = O stretching mode of $^{13}CO_2$ at 2275 cm^{-1} was used. The values used were $A(2275\,cm^{-1}) = 7.8 \times 10^{-17}$ cm $molec^{-1}$ for mixtures without H_2O, $A = 7.6 \times 10^{-17}$ cm $molec^{-1}$ for mixtures containing less than 33% H_2O, and $A = 6.2 \times 10^{-17}$ cm $molec^{-1}$ for H_2O-dominated samples. These calculations were then used to determine the exact ratios of the respective mixtures in the ices.

3. RESULTS

Spectra in the 550–730 cm^{-1} range along with some specific peak positions and FWHM of the entire 658 cm^{-1} feature from experiments in Table 1 can be found on the University of Alabama at Birmingham Web site.[3] "Peak 1" refers to the subfeature of CO_2 at the higher wavenumber and "Peak 2" refers to the subpeak at the lower wavenumber. Some gas-phase CO_2 peaks such as the feature at 671 cm^{-1} were visible in many of

[3] http://www.phy.uab.edu/labastro

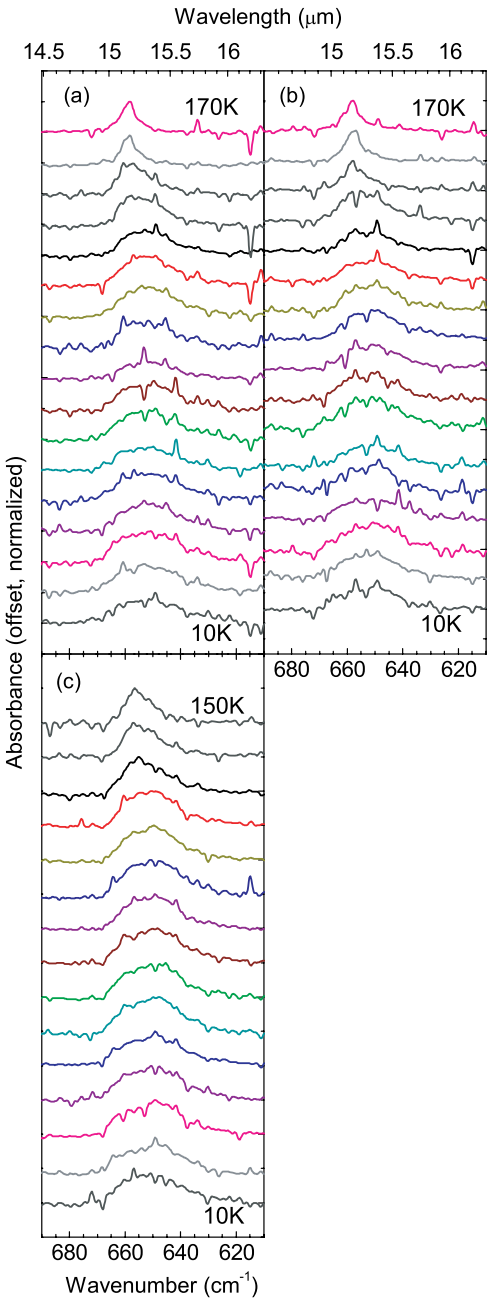

Figure 6. IR spectra, from 690 to 610 cm^{-1} (14.5 to 16.3 μm), of a laboratory ice mixture containing H_2O, CH_3OH, and CO_2 with more than 33% H_2O. All ice samples were heated at 1 K $minute^{-1}$ from 5 K to evaporation. Temperature intervals of 10 K are shown. (a) H_2O + CH_3OH + CO_2 (11:1.9:1), (b) H_2O + CH_3OH + CO_2 (12:3:1), and (c) H_2O + CH_3OH + CO_2 (8:7.7:1).

(A color version of this figure is available in the online journal.)

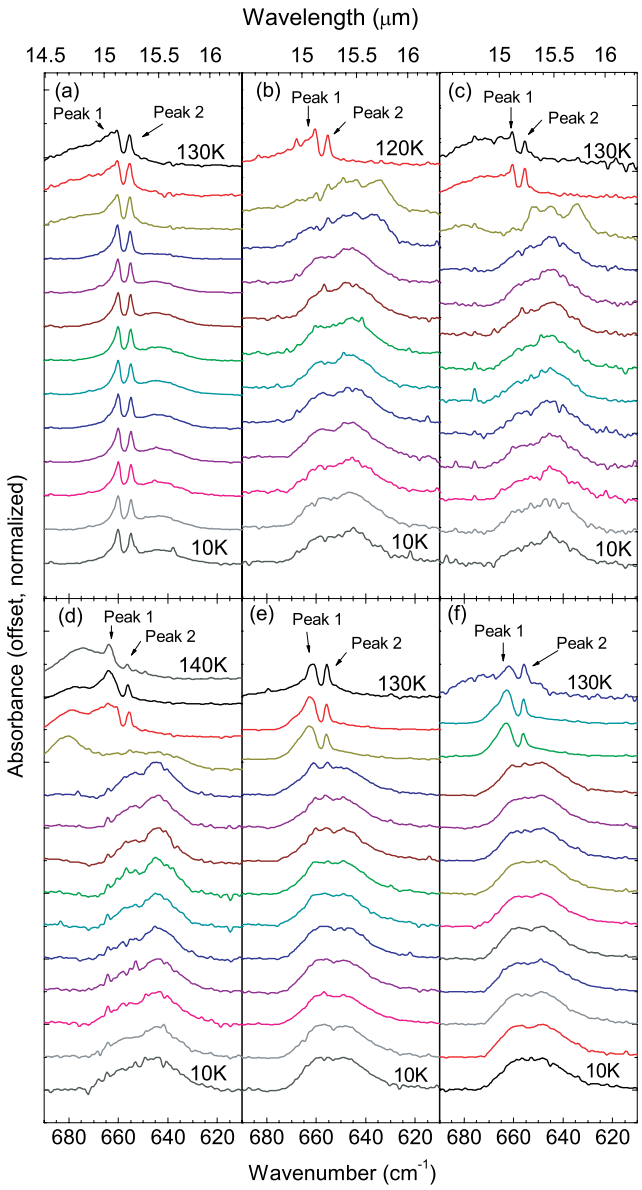

Figure 7. IR spectra, from 690 to 610 cm^{-1} (14.5 to 16.3 μm), of a laboratory ice mixture containing H_2O, CH_3OH, and CO_2 with more than 33% CH_3OH. All ice samples were heated at 1 K $minute^{-1}$ from 5 K to evaporation. Temperature intervals of 10 K are shown. (a) CH_3OH + CO_2 (2.9:1), (b) CH_3OH + CO_2 (2.1:1), (c) CH_3OH + CO_2 (6.7:1), (d) CH_3OH + CO_2 (13:1), (e) H_2O + CH_3OH + CO_2 (1:1.4:1), and (f) H_2O + CH_3OH + CO_2 (1:1.7:1). In experiments with at least 30% CH_3OH, a broad peak appeared at 680 cm^{-1} (14.7 μm) around 110 K.

(A color version of this figure is available in the online journal.)

the experiments, as well as small, sharp peaks within the spectra that were due to noise or an imperfect purge in the spectrometer.

3.1. CO_2-Rich Mixtures

Figure 2 contains the spectra of ice mixtures composed of H_2O, CH_3OH, and CO_2 with CO_2 concentrations of 33% or more in the range between 690 and 610 cm^{-1}, warmed up at 1 K $minute^{-1}$ from 10 K until evaporation (~120–130 K). In the H_2O + CO_2 (1:1) mixture, the 658 cm^{-1} feature appears as a single, broad peak at 656 cm^{-1} with a width of about 20 cm^{-1}. The 660 cm^{-1} subpeak of CO_2 appeared near 70 K as the width of the peak(s) decreased while the temperature increased. With temperatures below 70 K, the profile remained relatively unchanged from that measured at the lowest temperature. In mixtures with lower concentrations of CH_3OH (<50%), the double peaks of CO_2 were typically visible at the lowest temperature and remained visible until evaporation. The appearance of these mixtures varied, however, since the double-peak feature was intermittently visible as the temperature increased. At 35 K, the H_2O + CH_3OH + CO_2 (0.9:0.5:1) spectrum revealed a small peak at 649 cm^{-1} (Figure 2). This is consistent with observations of ice mixtures containing CH_3OH, since a peak near this position usually appeared at lower temperatures (10–40 K) as the ice was heated.

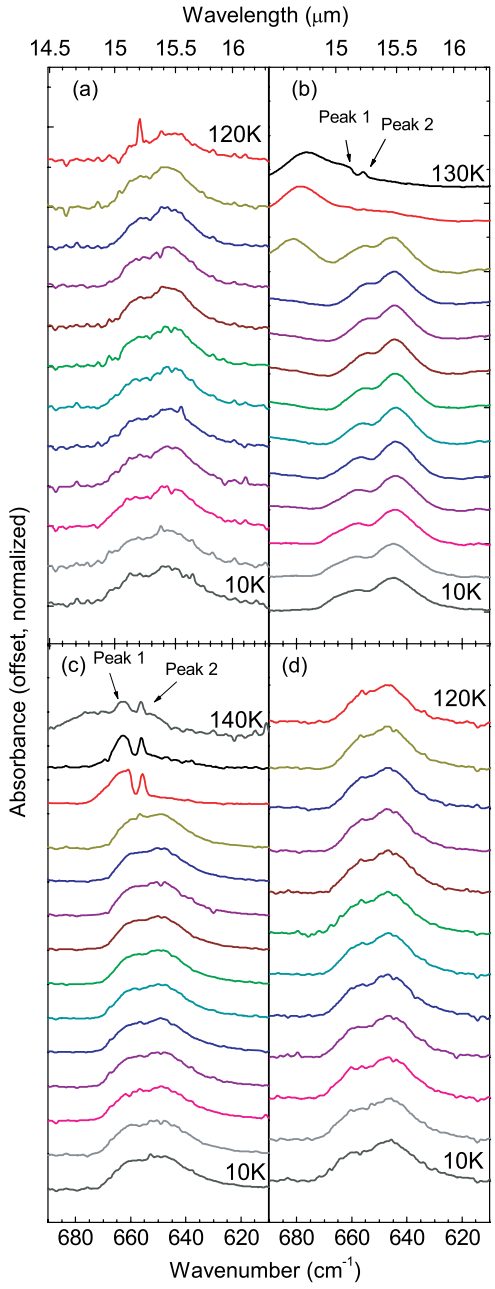

Figure 8. IR spectra, from 690 to 610 cm^{-1} (14.5 to 16.3 μm), of a laboratory ice mixture containing H_2O, CH_3OH, and CO_2 with more than 33% CH_3OH. All ice samples were heated at 1 K $minute^{-1}$ from 5 K to evaporation. Temperature intervals of 10 K are shown. (a) H_2O + CH_3OH + CO_2 (1.4:5:1), (b) H_2O + CH_3OH + CO_2 (2.4:11:1), (c) H_2O + CH_3OH + CO_2 (1.5:2.1:1), and (d) H_2O + CH_3OH + CO_2 (2.3:5.8:1).

(A color version of this figure is available in the online journal.)

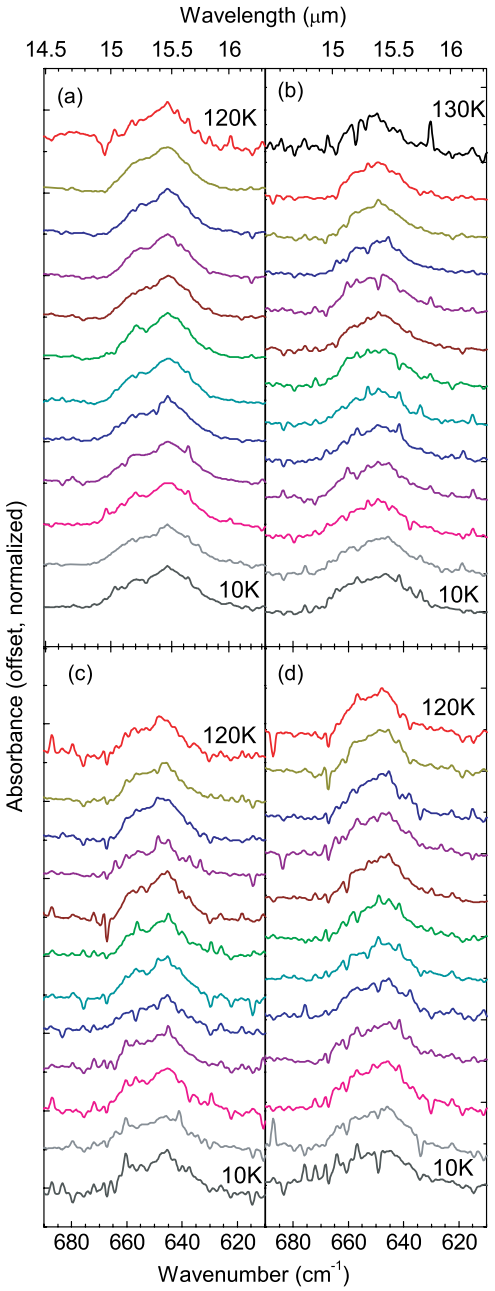

Figure 9. IR spectra, from 690 to 610 cm^{-1} (14.5 to 16.3 μm), of a laboratory ice mixture containing H_2O, CH_3OH, and CO_2 with more than 33% CH_3OH. All ice samples were heated at 1 K $minute^{-1}$ from 5 K to evaporation. Temperature intervals of 10 K are shown. (a) H_2O + CH_3OH + CO_2 (3.1:11:1), (b) H_2O + CH_3OH + CO_2 (5.3:8.8:1), (c) H_2O + CH_3OH + CO_2 (7.9:20:1), and (d) H_2O + CH_3OH + CO_2 (10:17:1).

(A color version of this figure is available in the online journal.)

3.2. H_2O-Rich Mixtures

In ice mixtures containing mostly H_2O ($\geqslant$ 33%), the CO_2 bending mode at the lowest temperature typically appeared as a single feature peaking at 656 cm^{-1} with an FWHM of 23–25 cm^{-1}. Figures 3–6 contain spectra of the H_2O-dominated mixtures. As in the case of H_2O + CH_3OH + CO_2 (1:0.9:1; Figure 3), the profiles below 70 K appear as two broad peaks. Above 70 K, the subpeaks of the double-peak structure appear at 660 and 655 cm^{-1}. The feature at 650 cm^{-1} remained but grew weaker until evaporation above 150 K. The peak positions shifted by as much as 9 cm^{-1} as the ice was warmed from the lowest temperature to evaporation.

Other experiments showed similar results, such as the spectra from a mixture of H_2O + CH_3OH + CO_2 (2.2:1.5:1) shown in Figure 4. A single peak at around 650 cm^{-1} was present with an FWHM of about 30 cm^{-1}. The broad feature at 650 cm^{-1} weakened above 110 K when the sharp 660 and 655 cm^{-1} peaks appeared. As in the case of the 1:0.9:1 mixture, at 120 K the width of the 660 cm^{-1} peak broadened slightly, by as much as 5 cm^{-1}, due to the appearance of the 680 cm^{-1} peak of CH_3OH. The FWHM of the two peaks, however, decreased by as much as 15 cm^{-1} as the temperature approached the evaporation point. At 110 K, the broad peak at 650 cm^{-1} present at the lowest temperature is seen as a weak shoulder overshadowed by the

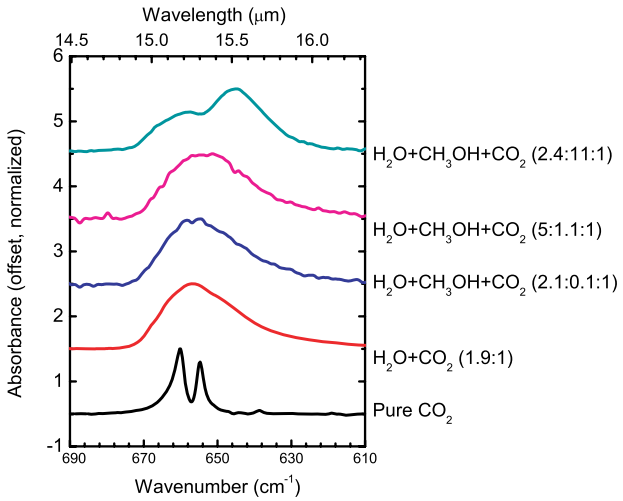

Figure 10. IR spectra of ice mixtures from 690 to 610 cm^{-1} (14.5 to 16.3 μm) at 10 K. The spectrum of pure CO_2 is shown for comparison.

(A color version of this figure is available in the online journal.)

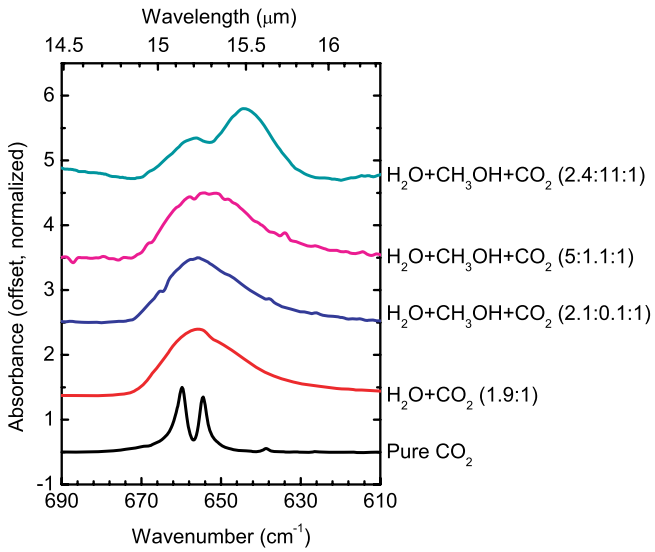

Figure 11. IR spectra from 690 to 610 cm^{-1} (14.5 to 16.3 μm) of laboratory ice mixtures taken at 50 K. The spectrum of pure CO_2 is shown for comparison.

(A color version of this figure is available in the online journal.)

much stronger 660 and 655 cm^{-1} peaks. The 655 cm^{-1} peak continued to sharpen and grow in relative strength until the ice evaporated around 135 K, while the 660 cm^{-1} peak tended to broaden and shift to about 662 cm^{-1}. Though the double-peak structure of the CO_2 bending mode was visible, broad shoulders remained on either side.

Only one peak was visible in mixtures containing 70% or more H_2O (Figure 6). It should be noted that because of interference from the strong, broad absorption feature due to the H_2O libration mode, the bending-mode feature of CO_2 was not visible in water-dominated mixtures when the ratio of H_2O:CO_2 was near 100:1. The libration mode of H_2O peaks at 770 cm^{-1} with a width of about 260 cm^{-1}.

3.3. CH_3OH-Rich Mixtures

Figures 7–9 contain 690–610 cm^{-1} spectra of mixtures dominated by CH_3OH (30% or more). At the lowest temperatures,

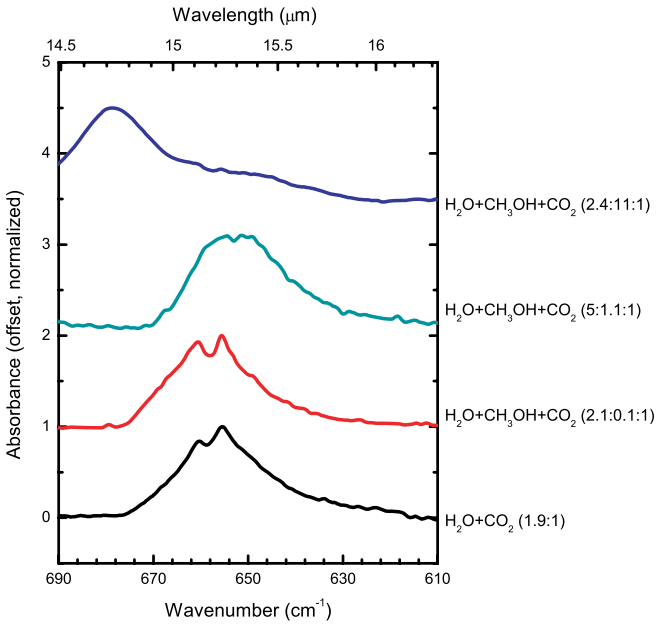

Figure 12. IR spectra from 710 to 610 cm^{-1} (14.1 to 16.3 μm) of laboratory ice mixtures at 120 K.

(A color version of this figure is available in the online journal.)

the profiles in these spectra typically appeared as two broad peaks. One peak is dominant at 647 cm^{-1} with a width of about 15 cm^{-1}, and the 658 cm^{-1} peak (with a width of about 15 cm^{-1}) is less prominent. Around 60 K the 658 cm^{-1} peak began to shift with each successive increase in temperature up to 75 K, when the same feature became centered at 655 cm^{-1}. At 110 K, a broad feature centered at 680 cm^{-1} appeared, which is characteristic of CH_3OH at this temperature. An experiment was performed with pure CH_3OH ice in order to verify this. The features at 655 and 647 cm^{-1} remained but grew much weaker as the ice reached 125 K, when only the 655 cm^{-1} peak was visible. Observations of these mixtures in this study are consistent with the spectral behavior of CH_3OH–CO_2 intermolecular complexes observed in previous studies and in theoretical calculations (Dartois et al. 1999; Klotz et al. 2004). When the sample contained more than 50% CH_3OH, the spectra exhibited only one absorbance peak near 649 cm^{-1} at the lowest temperature. At about 110 K, however, the double peak of CO_2 became visible at 660 and 655 cm^{-1}.

The $H_2O + CH_3OH + CO_2$ (2.4:11:1) mixture also provides a good example of the behavior of the 658 cm^{-1} feature. At 5.5 K, two broad features are present at 658 and 645 cm^{-1}. In this case, the 660 and 655 cm^{-1} features did not appear until the sample reached temperatures above 110 K. The $CH_3OH + CO_2$ (2.9:1) mixture, however, revealed some unexpected results. Unlike the other CH_3OH-dominated samples, the 660 and 655 cm^{-1} peaks of CO_2 were visible from the starting temperature until evaporation.

3.4. Discussion

Figure 10 contains examples of different concentrations of $H_2O + CH_3OH + CO_2$ ices at 10 K. Peak positions differ with composition, although the differences can be broadly grouped according to the dominant ice component. As compared to H_2O-dominated ices, mixtures containing at least 33% CH_3OH display a shift in the 658 cm^{-1} feature by about 10 to 15 cm^{-1},

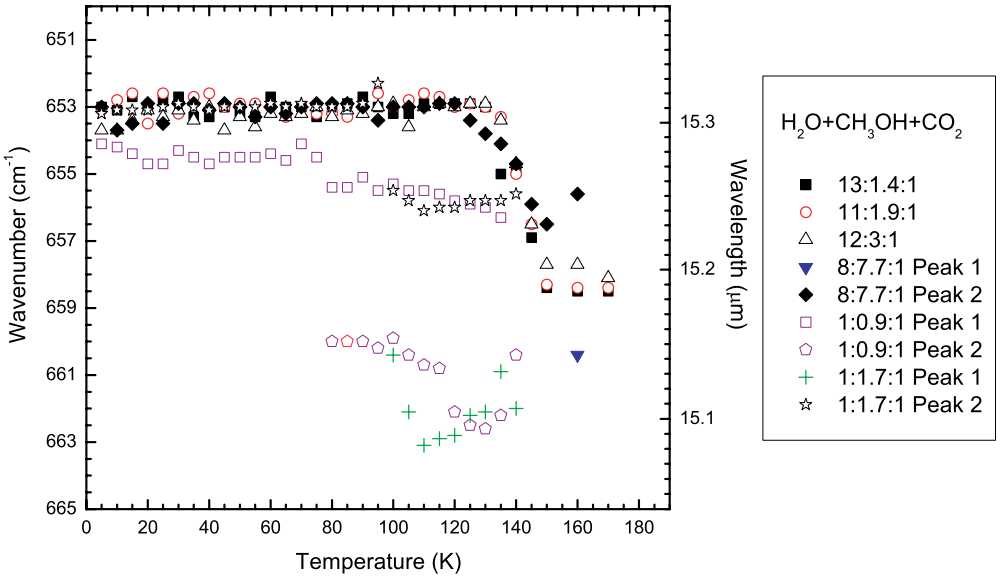

Figure 13. Peak position (in cm^{-1}) vs. temperature (in K) for various mixtures. "Peak 1" refers to the subfeature of CO_2 at the higher wavenumber and "Peak 2" refers to the subpeak at the lower wavenumber.

(A color version of this figure is available in the online journal.)

and a broadening by about 10 cm^{-1}. The same mixtures from Figure 10 (with the exception of CO_2) are shown in Figures 11 and 12 at 50 K and 120 K, respectively. From Figure 12, it is clear that the 658 cm^{-1} profiles change most dramatically as the mixtures approach their evaporation temperatures. As stated above, the 680 cm^{-1} feature of CH_3OH appears at temperatures above 110 K in mixtures with at least 33% CH_3OH. The double-peak structure of the CO_2 bending mode often did not appear until temperatures of about 120 K as in Figure 12, with the exception of H_2O-dominated mixtures (Figures 3–5) when the CO_2 features were very weak and did not appear until near the evaporation temperatures (above 150 K). The peak positions and widths of the CO_2 bending modes from each of the mixtures at different temperatures are listed in Table 1. CO_2 features were observed up to 160 K and 170 K in many experiments. This is most likely due to the well studied phenomenon of trapping within the water-ice matrix (Mastrapa et al. 2000; Ayotte et al. 2001). Water-ice deposited at low temperatures (<50 K) is amorphous in structure. As it is warmed above 140 K, water-ice undergoes a structural phase transition into a hexagonal crystalline form (e.g., the 2.2:1.5:1 mixture in Figure 3, and in the fitted spectra of Figure 14). During this reorganization of the matrix, any molecules diluted in the H_2O ice become mobile and may find new, lower-energy configurations. For CO_2, it has been shown that clusters of crystalline CO_2 form within the H_2O (Miller 1985). The growth of the sharp double-peaked structure of the 658 cm^{-1} feature and the shift of the stretching mode of $^{13}CO_2$ near 2282 cm^{-1} (4.38 μm) have each been used as evidence for this change in laboratory ice spectra.

General observations in this study may not be unique, since many of the characteristics of the CO_2 bending mode seen here have been documented in other experiments with different mixtures and different conditions (e.g., Ehrenfreund et al. 1999; Dartois et al. 1999; Gerakines et al. 1999; Klotz et al. 2004; Pontoppidan et al. 2008). However, the systematic documentation of ice mixture versus temperature provides a good foundation from which to examine ices in the ISM.

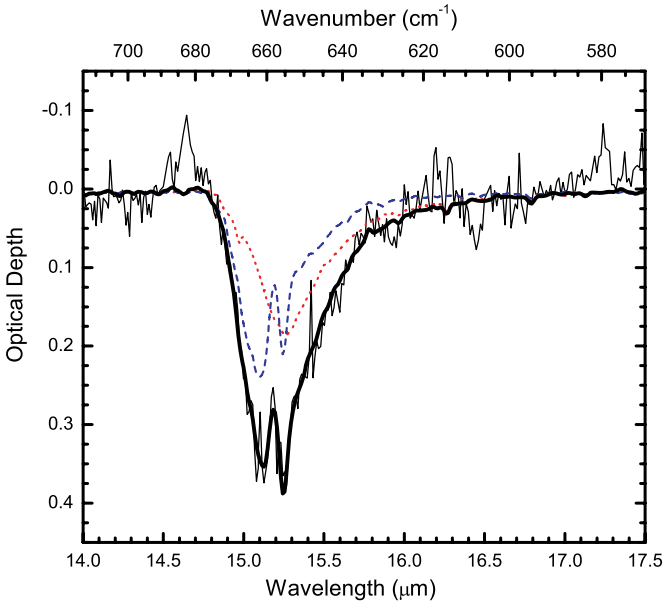

Figure 14. Absorption feature of interstellar solid CO_2 near 658 cm^{-1} of HH14, a low-luminosity object associated with IRAS 12553-7651 observed by *Spitzer* and fitted with laboratory spectra from this research. Short dashed line: laboratory spectrum of H_2O + CO_2 (6.7:1) at 75 K. Long dashed line: laboratory spectrum of H_2O + CH_3OH + CO_2 (2:0.9:1) at 125 K. Thin solid line: observed spectrum. Thick solid line: sum of components.

(A color version of this figure is available in the online journal.)

4. SAMPLE FITS TO OBSERVED PROFILES

The goal of the research described in this paper is to provide laboratory data for better interpretation of infrared observations of interstellar materials. Our systematic investigation of ice mixtures subject to thermal variations has resulted in a more extensive database for interpretation of observations than was

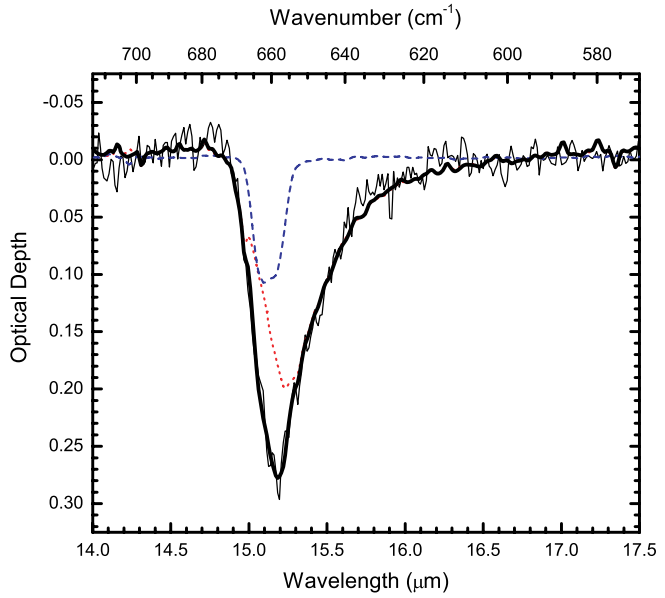

Figure 15. Absorption features of interstellar solid CO_2 near 658 cm^{-1} toward the Taurus Molecular Cloud in front of Elias 16 and fitted with laboratory spectra. Long dashed line: fit of a CO + O_2 + CO_2 (100:50:32) mixture at 10 K (from Ehrenfreund et al. 1997). Long dashed line: fit of the authors' H_2O + CO_2 (6.7:1) laboratory ice mixture at 25 K. Thin solid line: observed spectrum. Thick solid line: sum of components.

(A color version of this figure is available in the online journal.)

previously available. In this section, we present the results of fits to CO_2 features for two astronomical sources with contrasting properties: (1) a low-mass YSO still embedded in its birth envelope that provides an example of local heating of the ices in its environment, and (2) a field star that samples material in cold, quiescent regions of a dense cloud. All observations were obtained with the IRS of the *Spitzer Space Telescope* at a resolving power $R \sim 600$. The fits (shown in Figures 14 and 15) used a least-squares filling routine similar to that described by Gerakines et al. (1999).

HH14 (IRAS 12553-7651) is a low-mass pre–main-sequence star associated with an outflow and embedded in a dense clump in the Chameleon II cloud (Olmi et al. 1997). The optical depth spectrum between 790 and 570 cm^{-1} is shown in Figure 14: it displays a double-peaked CO_2 profile characteristic of ices heated to temperatures exceeding 90 K. Full details of the observations, including data reduction and analysis procedures and profile fitting, will be described in a future paper (A. M. Cook et al. 2009, in preparation). The profile is fitted with a combination of a polar ice (H_2O + CO_2 (6.7:1) at 75 K) and an annealed ice (H_2O + CH_3OH + CO_2 (2:0.9:1) at 125 K), the latter reproducing the sharp subfeatures in the spectrum. The data in Figure 14 suggest that the behavior of the CO_2 bending mode may offer insight into the temperature history of the ice by comparison to laboratory-generated spectra.

Elias 16 is regarded as a prototypical background field star with high extinction arising in the Taurus molecular cloud (e.g., Bergin et al. 2005; Knez et al. 2005; Whittet et al. 2007). The observed CO_2 bending-mode feature shown in Figure 15 is from Bergin et al. (2005). The fit to the profile indicates the presence of polar (H_2O-rich) and nonpolar (H_2O-poor) ices at low temperature, with polar ices dominating the mix. The structure associated with crystallization of the ices, apparent in the case of HH14 (Figure 14) is clearly lacking toward the field star, which is expected since the ices should not have undergone significant heating. The results of our fits to the CO_2 feature in Elias 16 are qualitatively consistent with those of previous authors to the CO_2 bending mode (Bergin et al. 2005; Knez et al. 2005), and also to the stretching mode (Gerakines et al. 1999).

We note in conclusion that the suite of laboratory analogues now available has resulted in satisfactory fits to the CO_2 bending mode in these objects (i.e., to within the scatter inherent in the observational data) with a fitting procedure that uses just two ice components (polar + nonpolar or polar + annealed). This may be contrasted with results reported by Pontoppidan et al. (2008), who invoke as many as five components to optimize their fits using a far more limited laboratory database. Of course, our results do not necessarily invalidate the results of Pontoppidan et al. (2008), but they do suggest that the level of complexity (and possible resultant ambiguity) associated with multicomponent fits may not be justified. Gerakines et al. (1999) previously suggested that features observed in laboratory spectra of ices heated to temperatures unlikely to be found in the ISM provide a good fit to much of the spectra received from IR observatories, as evident from the example fits in this study. This is not to assume that the ices observed are actually at these higher temperatures, but rather that the particular ice mixture observed may have been heated in its past by shock processing or annealing and then cooled. However, further research is needed to test whether two-component fits utilizing the extended laboratory database can adequately represent all the observed profiles.

This research was supported by NASA award NNG05GE44G under the Astronomy and Physics Research and Analysis (APRA) Program.

REFERENCES

Ayotte, P., Smith, S. R., Stevenson, K. P., Dohnalek, Z., Kimmel, G. A., & Kay, B. D. 2001, J. Geophys. Res. Planets, 106(E12):33, 387
Bergin, E. A., Melnick, G. J., Gerakines, P. A., Neufeld, D. A., & Whittet, D. C. B. 2005, ApJ, 627, L33
Boogert, A. C. A., et al. 2000, A&A, 353, 349
Chiar, J. E., Adamson, A. J., Kerr, T. H., & Whittet, D. C. B. 1995, ApJ, 455, 234
Dartois, E., Demyk, K., d'Hendecourt, L., & Ehrenfreund, P. 1999, A&A, 351, 1066
de Graauw, Th., et al. 1996, A&A, 315, L49
Ehrenfreund, P., Boogert, A. C. A., Gerakines, P. A., Tielens, A. G. G. M., & van Dishoeck, E. F. 1997, A&A, 328, 649
Ehrenfreund, P., Dartois, E., Demyk, K., & d'Hendecourt, L. 1998, A&A, 339, L17
Ehrenfreund, P., et al. 1999, A&A, 350, 240
Gerakines, P. A., Bray, J. J., Davis, A., & Richey, C. R. 2005, ApJ, 620, 1140
Gerakines, P. A., Schutte, W. A., Greenberg, J. M., & van Dishoeck, E. F. 1995, A&A, 296, 810
Gerakines, P. A., et al. 1999, ApJ, 522, 357
Gibb, E. L., Whittet, D. C. B., Boogert, A. C. A., & Tielens, A. G. G. M. 2004, ApJS, 151, 35
Gibb, E. L., et al. 2000, ApJ, 536, 347
Hagen, W., Allamandola, L. J., & Greenberg, J. M. 1979, Ap&SS, 65, 215
Hudgins, D. M., Sandford, S. A., Allamandola, L. J., & Tielens, A. G. G. M. 1993, ApJS, 86, 713
Hudson, R. L., & Moore, M. H. 1999, Icarus, 140, 451
Klotz, A., Ward, T., & Dartois, E. 2004, A&A, 416, 801
Knez, C., et al. 2005, ApJ, 635, L145
Mastrapa, R. M. E., Brown, R. H., Cohen, B. A., Anicich, V. G., Dai, W., & Lunine, J. I. 2000, in Lunar and Planetary Science, XXXI, 31, 2020
Miller, S. L. 1985, in NATO ASIC Proc. 156, Ices in the Solar System, 59
Moore, M. H., Hudson, R. L., & Gerakines, P. A. 2001, Spectrochemica Part A, 57, 843
Oberg, K. I., Fraser, H. J., Boogert, A. C. A., Bisschop, S. E., Fuchs, G. W., van Dishoeck, E. F., & Linnartz, H. 2007, A&A, 462, 1187

Olmi, L., Felli, M., & Cesaroni, R. 1997, A&A, 326, 373
Pontoppidan, K. M., et al. 2008, ApJ, 678, 1005
Sandford, S. A., & Allamandola, L. J. 1990, ApJ, 355, 357
Tielens, A. G. G. M., Tokunaga, A. T., Geballe, T. R., & Baas, F. 1991, ApJ, 381, 181
Watson, D. M., et al. 2004, ApJS, 154, 391
Weaver, H. A., Feldman, P. D., McPhate, J. B., A'Hearn, M. F., Arpigny, C., & Smith, T. E. 1994, ApJ, 422, 374
Whittet, D. C. B., & Duley, W. W. 1991, A&AR, 2, 167
Whittet, D. C. B., Shenoy, S. S., Bergin, E. A., Chiar, J. E., Gerakines, P. A., Gibb, E. L., Melnick, G. J., & Neufeld, D. A. 2007, ApJ, 655, 332
Whittet, D. C. B., et al. 1998, ApJ, 498, L159